AIAA 94-1801
Integrated Tail Buffet Loads on the F/A-18

Larry A. Meyn
NASA Ames Research Center, Moffett Field, CA

Kevin D. James
Sterling Federal Systems, Inc., Palo Alto, CA

12th AIAA Applied Aerodynamics Conference

June 20-22, 1994 / Colorado Springs, CO

Integrated Tail Buffet Loads on the F/A-18

Larry A. Meyn*
NASA Ames Research Center, Moffett Field, California 94035
and
Kevin D. James†
Sterling Federal Systems, Inc., Palo Alto, California 94303

ABSTRACT

The unsteady pressures acting on the vertical tails of a full-scale F/A-18 fighter aircraft were studied to gain a better understanding of tail-buffet loads that frequently occur on fighter aircraft operating at high angles-of-attack. Data for the study were acquired during two test entries in the 80- by 120-Foot Wind Tunnel wherein the aircraft was tested at wind speeds up to 100 knots and at angles-of-attack from 20° to 40°. For the purposes of this paper, the primary difference between the two tests is that, during the first wind-tunnel entry, the pressure transducers were more sparsely spaced and covered less of the fin than during the second entry. In addition to a brief description of the spectral analysis methods used for the unsteady aerodynamic pressures and loads, an analysis of the effects of sensor density on estimating integrated loads is presented. It was found that the integrated loads determined from sparse sensor arrays are significantly higher than actual loads. However, a modest increase in the number of sensors can greatly reduce the error and a method for correcting load estimates from sparse sensor arrays is also suggested. The results for the time-averaged, power-spectral analysis are then presented for the tail-fin bending moments. Power spectra are presented for the aircraft at zero sideslip over an angle-of-attack range from 20° to 40° and for the aircraft at an angle-of-attack of 30° over a sideslip range from -16° to 16°. Since the aircraft was equipped with a removable leading-edge extension (LEX) fence to reduce tail-buffet loads, the tail-fin bending moment loads are also presented for that configuration. The LEX fence is shown to significantly reduce bending moment loads over a broad range frequencies, for all the aircraft attitudes presented.

NOMENCLATURE

$\bar{c}$	mean aerodynamic chord (m.a.c.), 11.52 ft
$Re_{\bar{c}}$	Reynolds number based on m.a.c.
α	angle-of-attack, degrees
β	angle-of-sideslip, degrees
b	reference wing span, 37.42 ft
$C_{p''}$	pressure power coefficient, $\frac{4p''}{l\rho^2 V^3}$
f	frequency, Hz
K	reduced frequency, $f\bar{c}/U_\infty$
k	local reduced frequency, $f\ell/v$
ℓ	characteristic length
N	normal force on tail, lbs
p	pressure, psi
p''	unsteady pressure power, psi^2/Hz
q_∞	free-stream dynamic pressure, $\frac{1}{2}\rho V^2$, psf
ρ	density, 0.00237 slugs/ft^3
S	reference wing area, 400 ft^2
σ	standard deviation
σ^2	variance
T	sampling period, sec
t	time, sec
U_∞	free stream velocity, 168 ft/sec
v	wave speed, ft/sec
ω	frequency in radians/sec, $2\pi f$

INTRODUCTION

Tail buffet and its associated structural fatigue are a concern for any aircraft configuration where vortical flow shed from the forward portion of the aircraft passes close to the vertical tail(s). The F/A-18 configuration has wing leading-edge extensions (LEX) to provide high lift and to allow for high angle-of-attack maneuvers. In order to provide sufficient tail authority at low angles-of-attack, the twin vertical tails were placed directly in a region occupied by the vortical flow that is shed by the forebody and LEX at high angles-of-attack. Tail buffet on the F/A-18 occurs when the turbulent flow from the burst vortices impinges on the twin vertical tails, with sufficient power, at the structural resonance frequencies. Operational experiences with the F/A-18 show that tail buffet and the resulting structural fatigue is a serious concern. In particular, the F/A-18 has a tail buffet problem at angles-of-attack above 26° and below 35°. A streamwise fence is mounted on the LEX's of operational F/A-18 fighter aircraft to reduce the buffet problem (Fig. 1).

Tail buffet measurements on a production F/A-18 were made during two full-scale tests in the 80- by 120-Foot Wind Tunnel. This paper provides an overview of the bending moment loads due to tail buffet that are based on data acquired during the second full-scale test conducted on a production F/A-18 aircraft. Tail buffet data were acquired over an angle-of-attack range of 20° to 40°, for a sideslip range of -16° to +16°, at wind speeds up to 100 knots, and with various forebody vortex control methods employed. The major differences between the first and second tests involve the spatial density of the pressure

*Aerospace Engineer. Member AIAA.

†Aerospace Engineer. Member AIAA.

transducers on the vertical tails and the data acquisition rates.

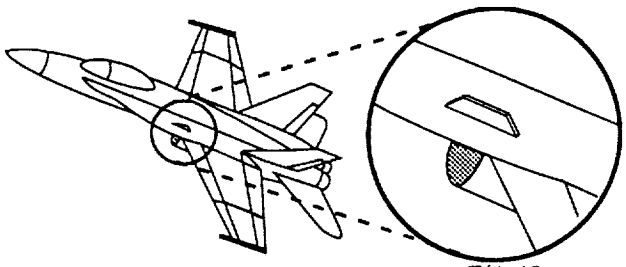

Fig. 1 LEX fence placement on F/A-18

There were three principle objectives of the full-scale F/A-18 tests. The first objective was to understand how angle-of-attack and sideslip affect tail buffet loads on twin-tailed aircraft. The data are being used to determine tail loading conditions for full-scale structural fatigue tests of the F/A-18[1]. The second objective was to understand why the LEX fence reduces tail-buffet loads. This information could lead to the development of alternative methods to reduce tail buffet loads. The other main objective was to aid in the development of guidelines to quantitatively predict tail buffet loads in flight from small-scale wind tunnel data[2-6] and Navier-Stokes computations[7,8]. To address this third objective, pressure transducers were located on the full-scale aircraft in many of the same locations used in small-scale tests.

This paper presents results from the second full-scale F/A-18 tail buffet test, which was an extension and refinement of the first test. The first test provided substantial insight to the F/A-18 tail buffet problem, LEX fence effect, and data analysis techniques; however, it also indicated that there was insufficient spatial resolution from the transducers to accurately quantify the tail-fin flow field. Therefore, additional pressure transducers were installed for the second test to provide a higher spatial resolution for measurements of the flow field over the vertical tails. An analysis of the effect of sensor density on the estimate of integrated loads is presented in the section on analysis methods. Although a wide variety of test conditions were examined during the test, the results presented here only include angle-of-attack variations at zero sideslip and sideslip variations at an angle-of-attack of 30°. Data is presented for the F/A-18 with and without LEX fences.

EXPERIMENTAL SETUP

The 80- by 120-Foot Wind Tunnel is part of the National Full-Scale Aerodynamic Complex (NFAC) located at NASA Ames Research Center[9]. The NFAC can be configured as either a closed circuit wind tunnel with a 40- by 80-foot test section or an open circuit wind tunnel with an 80- by 120-foot test section. A schematic of the facility is shown in Fig. 2. The maximum dynamic pressure attainable in the 80- by 120-Foot Wind Tunnel is 33 psf, providing a maximum velocity of approximately 100 knots. The wind tunnel is driven by six 40-foot diameter, variable speed, variable pitch fans. Each fan is powered by a 22500 hp electric motor and at full speed the wind tunnel draws 106 MW of power. The turbulence intensity in the test section is less than 0.5% at maximum dynamic pressure.

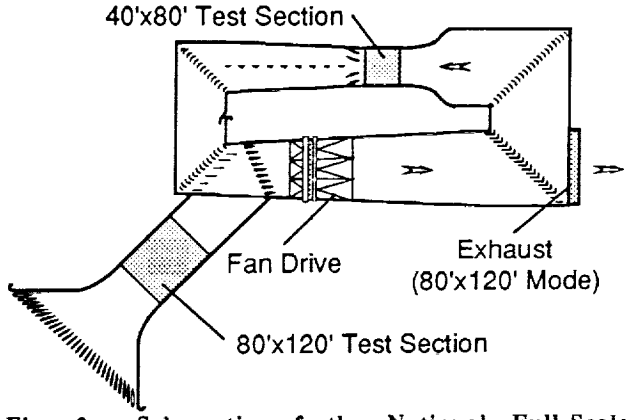

Fig. 2 Schematic of the National Full-Scale Aerodynamic Complex.

The aircraft was supported in the wind tunnel test section by the three struts shown in Fig. 3. The two, fixed height, main struts were connected by a horizontal cross-bar. The aircraft was attached to the cross-bar with two blade-and-clevis assemblies that replaced the main landing gear trunnions. The tail strut is a large linear actuator that pitches the aircraft about the main strut attachment pivots. In order to maintain a positive mechanical advantage at higher angles of attack, it was necessary to attach the tail strut to a point aft of the aircraft. This attachment configuration was achieved with a cantilevered structure connected to the F/A-18 engine mounts and to the arresting hook pivot.

The three struts were mounted on a turntable that is supported by a six-component scale system. Each strut is shielded from the flow by an aerodynamic fairing mounted on a non-metric turntable that tracks the balance turntable. The fairings rotate to stay aligned with the wind tunnel axis when the turntable rotates to yaw the aircraft. The fairing for the tail strut changes length and tilt angle to follow the tail strut when it is extended or retracted to pitch the model.

Test Article

The aircraft, acquired from the U.S. Navy, is from the first F/A-18 model A production block. The engines and avionics were removed prior to shipment to Ames Research Center. The aircraft is 56.0 ft long, has a wing span of 37.42 ft, a reference wing area of 400 ft^2, and a mean aerodynamic chord of 11.52 ft. The aircraft was mounted slightly below the centerline of the test section to reduce the effect of ceiling proximity on the forebody at high angles-of-attack. Wind tunnel blockage at 20° angle-of-attack is 4.9% and increases to 7.5% for an angle-of-attack of 50°.

The aircraft was configured with flow-through inlets. The aircraft missile rails were left in place; however, no missiles were attached. The aircraft had removable LEX fences, Fig. 1, which are installed on all U.S. Navy F/A-18 aircraft to reduce tail buffet loads. The LEX fences are trapezoidal in shape, 8.375 inches high, 36.6 inches long at the base, and 27.9 inches long at the top.

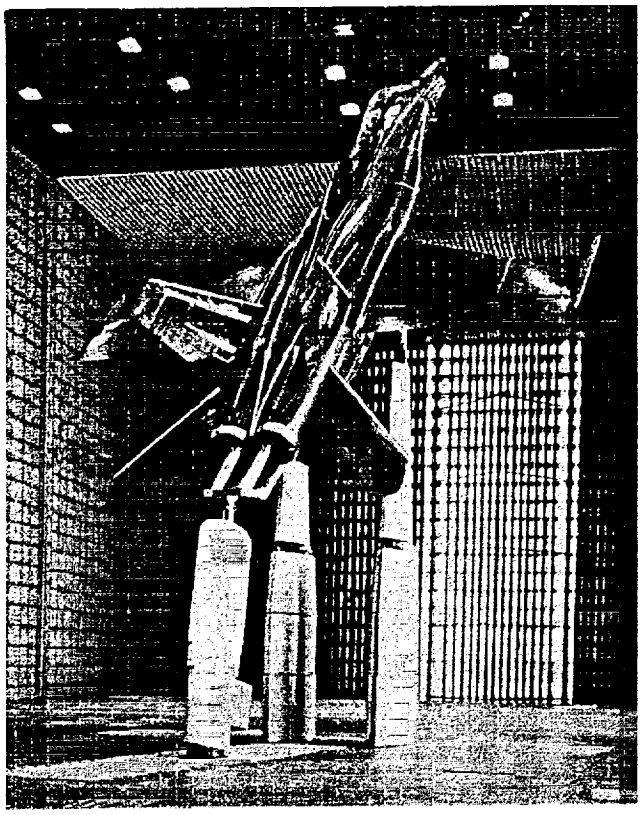

Fig. 3 F/A-18 in the 80- by 120-Foot Wind Tunnel.

The leading-edge flaps were fixed at a -34° deflection angle and trailing-edge flaps were fixed in their undeflected position. These flap deflections match the standard control-law schedule for angles-of-attack greater than 26°. The rudders were fixed in their undeflected position. The horizontal stabilators were actuated and their position was varied with angle-of-attack to match the trimmed stabilator positions of a typical flight line F/A-18 in steady, 1 "g" flight conditions.

Instrumentation

The tail-buffet instrumentation for the first full-scale test consisted of thirty-two 15 psia pressure transducers, eight accelerometers, six strain gages, and a surface temperature sensor. The pressure transducers were mounted on the surface of the left vertical tail in a four by four matrix on both the inboard and outboard surfaces, Fig. 4. A complete description is provided in References 10 and 11.

The second test tail buffet instrumentation consisted of ninety-six 15 psia pressure transducers, eight accelerometers, six strain gages, a surface temperature sensor, and two additional 15 psia pressure transducers, one located on the forward section of each LEX. The pressure transducers were mounted on the surface of the left vertical tail in a six by eight matrix on both the inboard and outboard surfaces, Fig. 4. Each vertical tail and each horizontal stabilator had two accelerometers mounted at their tips near the leading and trailing edges. The strain gages were attached to the attachment stubs of the two vertical fins and the temperature sensors were attached the surface of the left vertical fin.

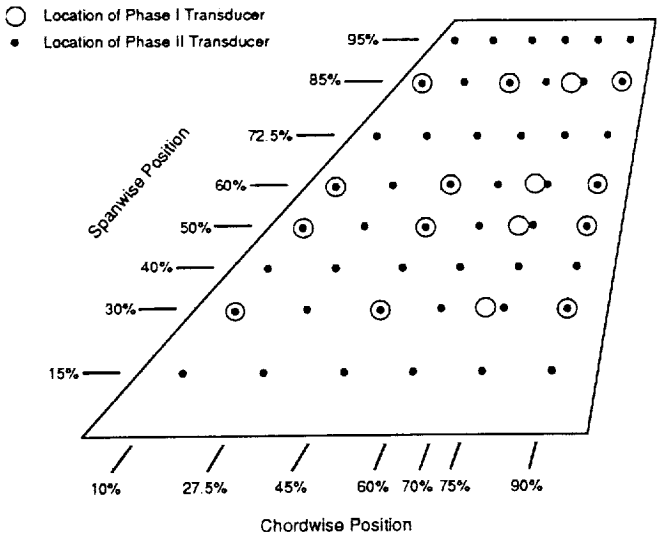

Fig. 4 Pressure transducer locations on F/A-18 port vertical fin.

The data sampling rate for the first test entry was 512 Hz per channel for a period of 32 seconds. For the second entry the sampling rate was 260 Hz per channel for periods up to 300 seconds. To eliminate concerns about damping due to pressure lines and to ease transducer installation, absolute pressure transducers, that did not have reference pressure lines, were installed on the tail surface. Fairings, depicted in Fig. 5, were mounted around each pressure transducer to eliminate pressure disturbances due to the transducers obstructing the flow. To eliminate any aliasing of the data, 100 Hz low-pass resistive filters were used to condition the signals prior to

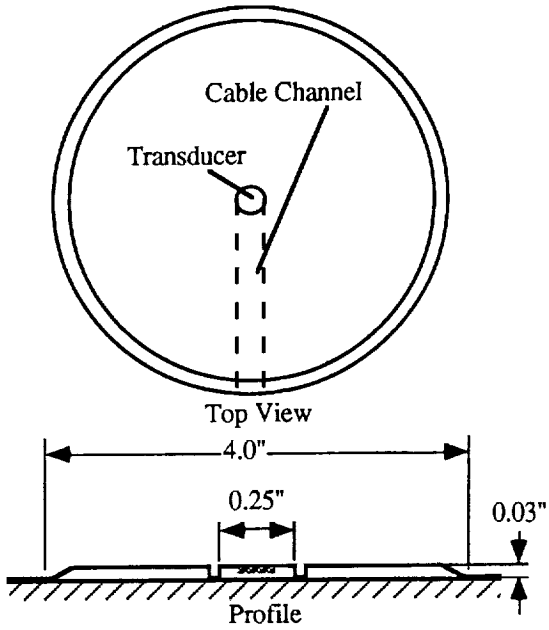

Fig. 5 Pressure transducer fairing

digital collection and storage. The signals from the pressure transducers were then routed to two separate amplifiers. One amplifier was A/C coupled to eliminate the large D/C offset due to atmospheric pressure and thereby allow greater signal gain for increased resolution of the unsteady pressures. The second amplifier was configured to record the D/C offset.

Ground Vibration Tests

Prior to the initial full-scale F/A-18 test, ground vibration tests were conducted on the aircraft and on the vertical fins to determine if the bending modes and natural frequencies were affected by the lack of engines and by mounting the aircraft on struts. These tests were conducted by a team from the U.S. Air Force Wright Research Laboratory.[12] Ground vibration tests were performed on the aircraft both on the ground and mounted on the wind tunnel struts. The vertical fin had the first structural bending mode at 15 Hz, the second bending mode at 61 Hz, and the first torsion mode at 43 Hz; these measured values are close to those measured on a fully configured production aircraft.

Test Conditions

A majority of the data for both tests were acquired at a free stream velocity of 168 ft/s. This velocity corresponds to a dynamic pressure of 33 psf, a Mach number of 0.15, and a Reynolds number of 12.3 million based on mean aerodynamic chord. The lowest velocity tested in the second entry was 130 ft/s, which corresponds to a dynamic pressure of 20 psf. The angle-of-attack ranged from 20° to 40° and the sideslip angle ranged from -16° to 16°.

ANALYSIS METHODS

Data Reduction

The method chosen to estimate the power spectral distribution (PSD) for both test entries was a single-sided periodogram utilizing a Fast-Fourier-Transform algorithm (ref. 13.) This is a classical method of PSD estimation, and it has the advantage that the integral of the estimated PSD with respect to frequency is equal to the variance (or the RMS^2) of the signal. Details for the data reduction in the first test are given in reference 11. In order to determine time-averaged PSD's for the 300 second data records in the second entry, each record was subdivided into 1221 half-second time records that overlapped by 50%. A Hann window[13] was applied to each record, which contained 128 samples, and then each record was padded with zeros to increase the record length to 4096. PSDs were calculated for each record and averaged to yield a time-averaged PSD. The standard deviation of the PSD's is estimated to be 3%, based on the number of averages used. This would correspond to an error band of ±6%.

Differential pressures were calculated by subtracting the inboard pressure value from the corresponding outboard pressure at each time step. Bending moments due to buffet pressure were calculated by first dividing the surface area of the vertical fin as shown in Fig. 6. Then the differential pressures measured at the transducer locations shown were multiplied by the area of the enclosing sub-area. These forces were then multiplied by the distance of the sub-area centroid from the fin root. To compute the torsional bending moment, these forces were multiplied by the distance of the sub-area centroid from the 55% local chord value. The values for all 48 sub-areas were then summed for each time step to obtain a time history for the bending moment imposed by the pressure field on the fin.

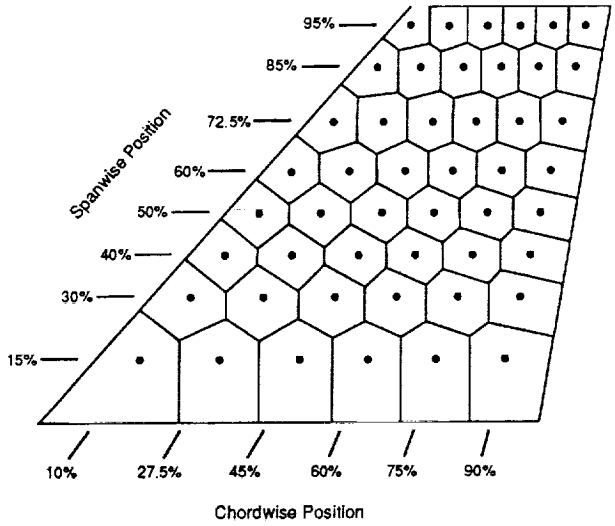

Fig. 6 Sub-section areas surrounding pressure transducers on tail.

Non-Dimensional Parameters

The derivations of non-dimensional parameters for frequency and buffet pressure PSDs are given in Reference 1. The definitions for the non-dimensional frequency, K, and the PSD pressure coefficient, C''_p, are given in the nomenclature and use the mean aerodynamic chord (11.52 ft) for the characteristic length scale and the free stream velocity, U_∞, was chosen as the characteristic velocity. In addition, it is also useful to define a local non-dimensional frequency, k, that is based on a local length scale, ℓ, and a wave propagation speed, v. The wave speed was chosen to be $0.45U_\infty$, which is consistent with the F/A-18 tail fin wave propagation speed reported in Reference 6.

Integrated Loads as a Function of Sensor Density

In an earlier paper[14], the bending moment power from the first full-scale F/A-18 wind tunnel test was shown to be as much as 60% higher than the bending moment power from the second test. Part of this discrepancy can be attributed to the use of shorter time records in the first test, which yielded power spectra with estimated errors of ±18% (±2σ.), three times the estimated error for the second test. However, most of the discrepancy between the two results was attributed to the limited number of sensors used on the vertical tail in the first test. This was confirmed when the bending-moment power in the second test was calculated using only the sensors at locations used in the first test. The resulting

bending-moment powers using the sparse sensor array were as much as 30% higher than the bending moment powers determined from the full sensor array.

Given the large differences in integrated load estimates between the two array densities, the question arises as to how dense an array is needed to get accurate load estimates. To answer this question, a simplified analytical model of the physics was studied. Figure 7 shows the relevant dimensions for a flat plate that is subjected to a pressure wave traveling in the x or streamwise direction. The pressure wave is assumed sinusoidal and continuous along the length of the flat plate; however, sensors on the plate only measure this pressure at discrete points. The integrated loads estimated from the discrete sensors assumes that the measured pressure at the sensor location is applied over the entire sub-area surrounding the sensor. Equation 1 describes the variance of the integrated normal force due to a sinusoidal pressure wave for the continuous response of the flat plate. Equation 2 gives the discrete response of an array of N sensors. The pressure wave has a frequency of ω, an amplitude of $p(\omega)$, and a wave velocity of v.

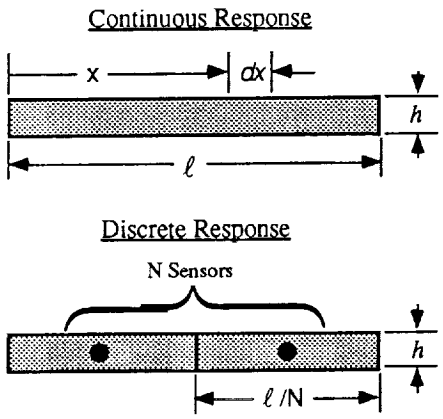

Fig. 7 Geometry for a simplified model of how a plate responds to a pressure wave traveling in the x direction.

$$\sigma^2[N(w)] = \lim_{T\to\infty}\frac{1}{T}\int_0^T\left(\int_0^\ell p(w)\sin\left(wt + w\frac{x}{v}\right)h\,dx\right)^2 dt \quad (1)$$

$$\sigma^2[N(\omega,i)] = \lim_{T\to\infty}\frac{1}{T}\int_0^T\left(\sum_{i=0}^{N-1} p(\omega)\sin\left(\omega t + \frac{\omega\ell}{vN}\left(i+\tfrac{1}{2}\right)\right)\frac{\ell}{N}h\right)^2 dt \quad (2)$$

Equation 1 has a closed form solution that is given in equation 3. Recasting this equation in terms of the non-dimensional frequency, k, and then normalizing to give the variance in force for a unit amplitude pressure wave applied over a unit area plate yields equation 4.

$$\sigma^2[N(\omega)] = \frac{v^2h^2}{\omega^2}\left(1-\cos\left(\omega\frac{\ell}{v}\right)\right)p(\omega)^2 \quad (3)$$

$$\sigma^2\left[\frac{N(k)}{p(k)\ell h}\right] = \frac{1-\cos(2\pi k)}{4\pi^2k^2} \quad (4)$$

Equation 2, for the integrated force variance estimated from discrete sensors was solved numerically and the results were non-dimensionalized and normalized in the same manner described above. The results for several sensor densities are shown in Figure 8, which is essentially a PSD frequency response curve.

The N =1 curve has a constant value of 0.5, which is the variance of a unit sine wave. The continuous flat plate response, labeled N = ∞, shows rapid attenuation of power as frequency is increased and shows little response to non-dimensional frequencies greater than 1. Surprisingly, the frequency response for four sensors is very close to the continuous case and the curve for eight sensors cannot even be distinguished from the N = ∞ curve at this scale. This analysis would imply that, in one dimension, eight sensors should yield very good estimates for integrated, unsteady normal force loads.

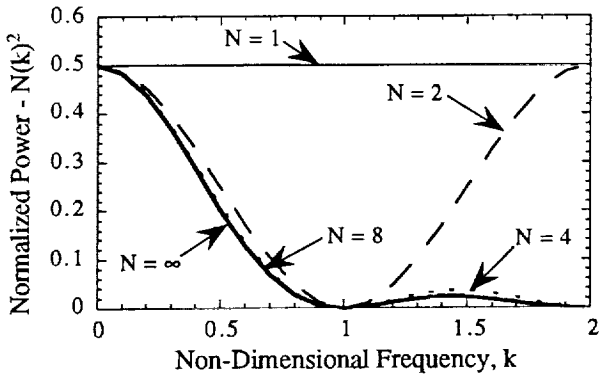

Fig. 8 Estimated normal force variation as a function of frequency for several sensor densities.

Unfortunately the pressure field in which the vertical tails are immersed is considerably more complicated than the uniform pressure field assumed in this simple pressure response model. Drawing conclusions from a model that assumes a uniform pressure field over the surface of the entire tail is somewhat suspect. A more reasonable approach would be to assume that the pressure field around each sensor is locally close to uniform. With this approach, the pressure field response for each sensor sub-area is being estimated by a single sensor. Division of the single sensor variance by the variance for a continuous flat plate yields a function that describes the gain for single sensor load estimates (Figure 9.) This shows that the gain rapidly increases as the local non-dimensional frequency, k, increases. For a given flow field, k is primarily a function of the local length scale, ℓ. So as sensor density increases, ℓ decreases, and the single sensor gain significantly decreases.

To compare the expected gains of the sensor arrays used in the two test entries with each other, a representative value of k for the estimated tail fin wave speed, 75 ft/s, the highest frequency containing significant power, 10 Hz, and the sensor sub-area dimensions is used.

For a sensor near the tip of the tail in the first test, k would range from 0.2 to 0.3, depending on whether the chordwise or spanwise dimension was used. This would correspond to gains from 1.16 to 1.36. For a sensor near the tip of the tail in the denser array that was used during the second test, the local k would be 0.1, which has a gain of only 1.035.

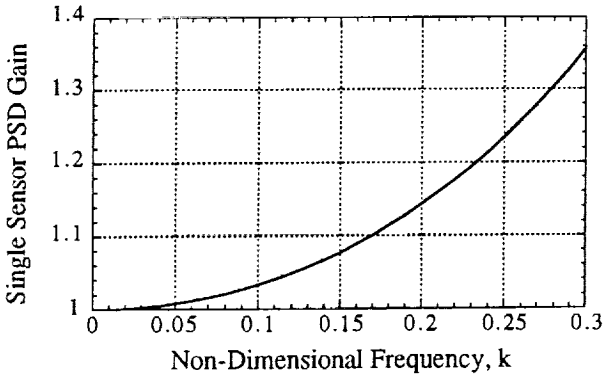

Fig. 9 The gain of a single sensor when used to estimate the PSD of forces on a flat plate.

The foregoing analysis led to the conclusion that the sparse sensor array in the first test would significantly over estimate power for unsteady loads and that the power estimates from the more dense sensor array used in the second test would only be a few percent too high. This analysis suggests a method to be used to determine more accurate integrated loads when only sparse arrays are available. First a transfer function could be determined for each sensor that would yield the estimated frequency response for the sensor sub-area. Then the pressure signal from each sensor can be run through the transfer function before loads are calculated.

EXPERIMENTAL RESULTS

The integrated-bending-moment results presented in this paper are for the dense sensor array on the port (left) vertical tail and only data records of 300 seconds in length were used. The two angle-of-attack sweeps presented here, for zero sideslip, are comprised of data record points at angles-of-attack of 20°, 24°, 26°, 28°, 30°, 32°, 34°,36°, and 40°. The two sideslip sweeps are, at an angle-of-attack of 30°, are comprised of data record points at sideslip angles of -16°, -10°, -6°, -4°, -2°, 0°, 2°, 4°, 6°, 10°, and 16°. All told, over 600 Mb of data were used to produce the figures shown here.

Figure 10 presents the bending-moment power as a function of non-dimensional frequency and the aircraft angle-of-attack. The Figure 10(a) presents the PSD's for the aircraft without a LEX fence. The region of the worst buffeting occurs for angles-of-attack from 28° to 34° and between frequencies of 0.35 and 0.6. The effect of the LEX fence can be seen in Figure 10(b). The LEX fence is shown to cut the bending-moment power over the entire range of frequencies and angles-of-attack. The highest bending-moment power attained with the LEX fence is less than half of what occurs without the LEX fence.

Figure 11 presents the bending-moment power as a function of non-dimensional frequency and sideslip angle for an angle-of-attack of 30°. The Figure 11(a) presents the PSD's for the aircraft without a LEX fence. The peak

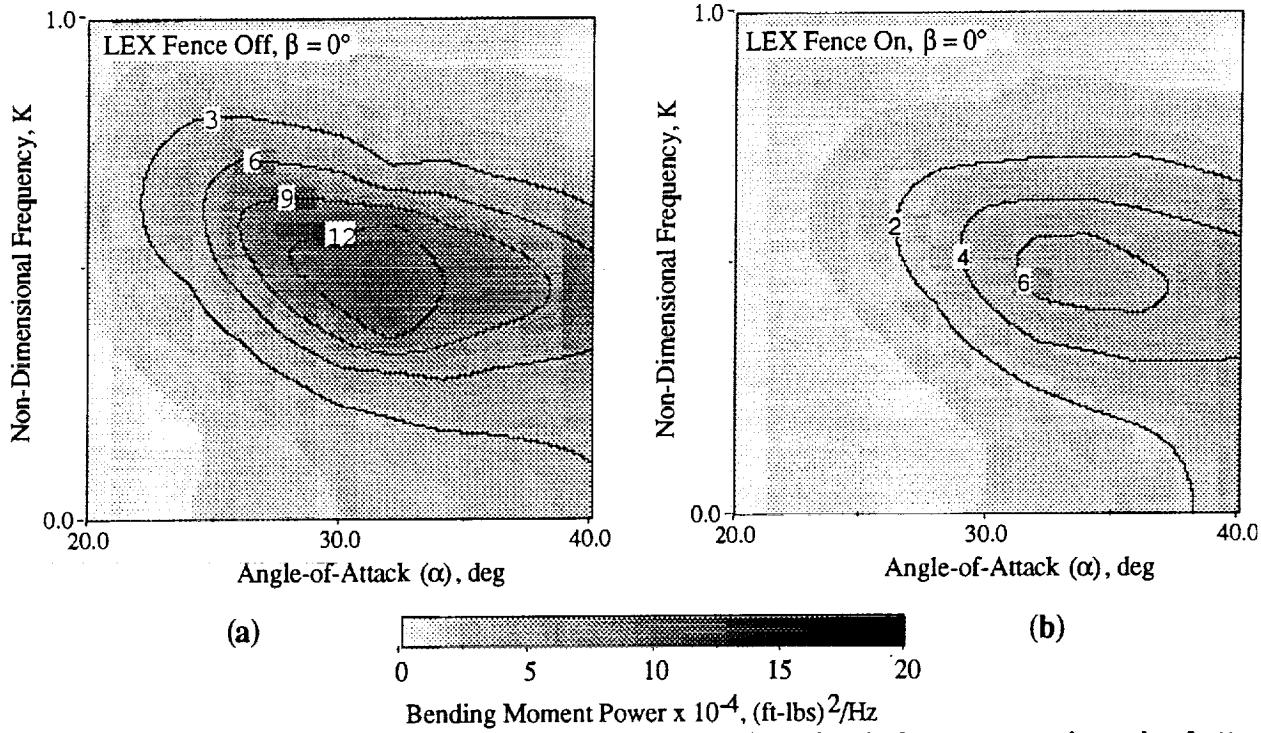

Fig. 10 Bending moment power as a function of non-dimensional frequency and angle-of-attack. Sideslip angle is 0°. (a) Without LEX fence installed. (b) With LEX Fence installed.

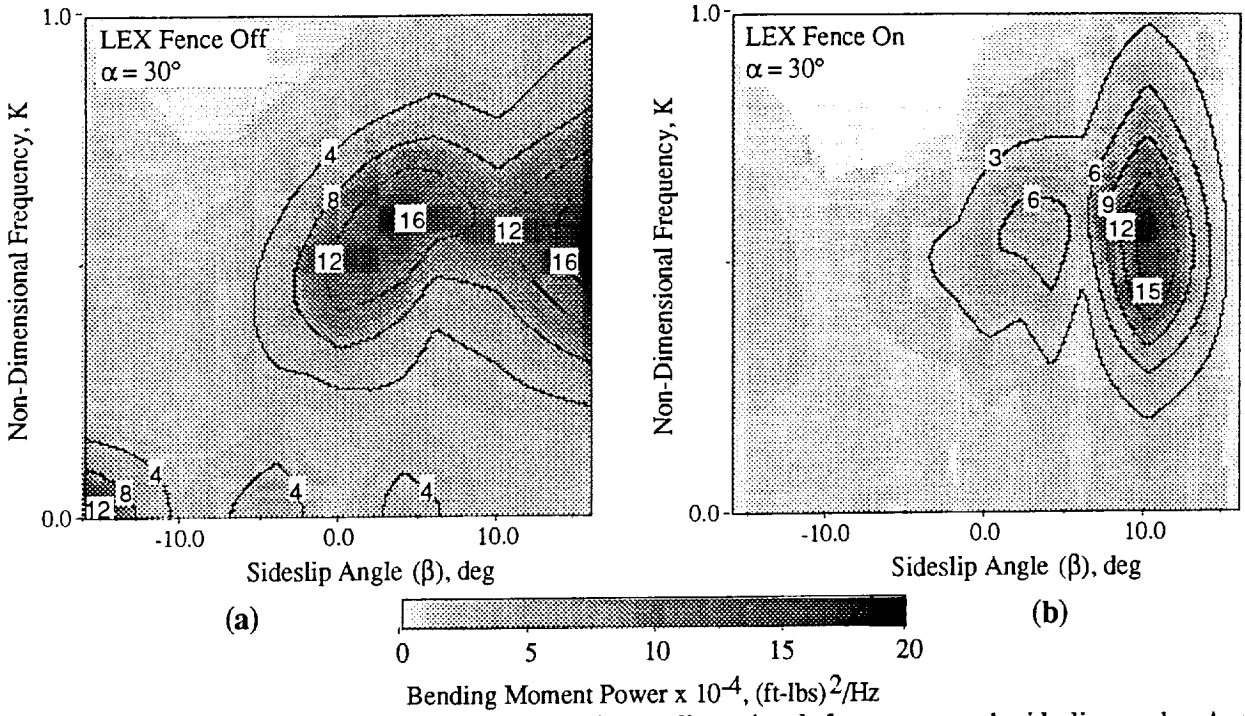

Fig. 11 Bending moment power as a function of non-dimensional frequency and sideslip angle. Angle-of-attack is 30°. (a) Without LEX fence installed. (b) With LEX Fence installed.

that occurs in the bending-moment power at $\beta = 4°$ (aircraft nose to the pilot's left,) is probably due the port LEX vortex being positioned so that it delivers more energy into the tail. The peak at $\beta = 16°$ is probably due to the starboard LEX vortex hitting the tail. An unexpected feature in the sideslip data is the low frequency power concentrations at $\beta = -16°$, -4°, and 4°. The source of these power concentrations is unknown, but they are probably of little concern since they occur at frequencies that are likely to be below structural frequencies. The effect of the LEX fence is shown in Figure 11(b). The two high power peaks at $\beta = 4°$ and 16° have been replaced by a slightly lower peak at $\beta = 10°$. The low frequency powerconcentrations evident in Figure 11(a) are not present. The LEX fence has a significant effect when the aircraft is yawed, but more study would be required to determine the physical process that causes the effects shown in this data.

CONCLUSIONS

Unsteady surface pressures on one of the vertical tails of a production F/A-18 aircraft, with and without a LEX fence, were measured during two test entries the 80- by 120-Foot Wind Tunnel. Data from the second test entry was used to estimate the unsteady bending-moment power imparted to the tail from the buffeting of the LEX vorticies. The unsteady bending-moment power is presented as a function of non-dimensional frequency for several aircraft orientations in both angle of attack and sideslip. The bending-moment power was shown to be greatest when the aircraft, without the LEX fence, was yawed to sideslip angles of 4° and 16°, angles which correspond to the vertical tail being in line with the port and starboard LEX vortices respectively. Results show that the LEX fence reduced bending-moment power by 50% when the aircraft was at zero sideslip. The LEX fence also reduced the bending-moment power when the aircraft was yawed, but a significant power concentration was evident at a sideslip angle of 10°. Overall, the LEX fence was shown to significantly reduce, for all aircraft attitudes, bending-moment power input to the tail from the LEX vorticies.

Because the two test entries of the F/A-18 had different sets of instrumentation, comparisons between the results of the two test were made. The first entry had a 4x4 array of pressure sensors on the tail and the second entry had a 6x8 array of sensors on the tail. The unsteady pressure measurements for sensors at any given location were in very good agreement between the two tests.[14] However, the integrated unsteady bending-moments derived from the 4x4 array of sensors in the first test were significantly larger than the bending-moments derived from the denser array of sensors used in the second test. When a 4x4 subset of the array used in the second test was used to calculate unsteady-bending-moment, a similar increase in the estimated unsteady bending-moments resulted. To explain the differences in estimated unsteady bending-moments, an analytic model of the effect of sensor density on estimating integrated loads is presented in this paper. This analysis shows that the sensor density used in the first test would lead to large over estimates of unsteady bending-moment. In contrast, the analysis shows that the sensor array used during the second test would result in an over estimation of the unsteady-bending-moment power of only a few percent. The analysis also provides direction as to how data from sparse sensor arrays might be used to determine more realistic integrated loads.

REFERENCES

1 Zimmerman, N.H. and Ferman, M.A.: "Prediction of Tail Buffet Loads for Design Application," NADC-88043-60, July 1987.

2 Martin, C.A.; Glaister, M.K.; MacLaren, L.D.; Meyn, L.A.; and Ross, J.: "F/A-18 1/9th Scale Model Tail Buffet Measurements," Flight Mechanics Report 188, Aeronautical Research Laboratory, Melbourne Australia, June 1991.

3 Shah, G.H.: "Wind-Tunnel Investigation of Aerodynamic and Tail Buffet Characteristics of Leading-Edge Extension Modifications to the F/A-18," AIAA Paper 91-2889, Atmospheric Flight Mechanics Conference, August 1991.

4 Shah, G.H.; Grafton, S.B.; Guynn, M.D.; Brandon, J.M.; Dansberry, B.E.; and Patel, S.R.: "Effect of Vortex Flow Characteristics on Tail Buffet and High-Angle-of-Attack Aerodynamics of a Twin-Tail Fighter Configuration," High-Angle-of-Attack Technology Conference, October 1990.

5 Lee, B.H.K. and Brown, D.: "Wind-Tunnel Studies of F/A-18 Tail Buffet," Journal of Aircraft, Vol. 29, No. 1, 1992, pp. 146-152.

6 Lee, B.H.K. and Tang, F.C.: "Characteristics of the Surface Pressures on a F/A-18 Vertical Fin Due to Buffet," Journal of Aircraft, Vol. 31, No. 1, 1994, pp. 228-235.

7 Rizk, Y.M. and Gee, K.: "Numerical Prediction Of The Unsteady Flowfield Around The F-18 Aircraft At Large Incidence," AIAA Paper 91-0020, 29th Aerospace Sciences Meeting, January 1991.

8 Rizk, Y.M.; Guruswamy, G.P.; and Gee, K.: "Computational Study of F-18 Vortex Induced Tail Buffet," AIAA Paper 92-4699, 4th Symposium on Multidisiplinary Analysis and Optimization, September 1992.

9 Corsiglia, V.R.; Olson, L.E.; and Falarski, M.D.: "Aerodynamic Characteristics of the 40- by 80/80- by 120-Foot Wind Tunnel at NASA Ames Research Center," NASA TM 85946, April 1984.

10 Meyn, L.A.; Lanser, W.R.; and James, K.D.: "Full-Scale High Angle-of-Attack Tests of an F/A-18," AIAA Paper 92-2676, 10th Applied Aerodynamics Conference, June 1992.

11 Meyn, L.A. and James, K.D.: "Full-Scale Wind Tunnel Studies of F/A-18 Tail Buffet," AIAA Paper 93-3519, 11th Applied Aerodynamics Conference, August 1993.

12 Levraea, V.J.; Henderson, D.A.; Pacia, A.P.; Banford, M.P.: "Modal Survey of a Full-Scale F-18 Wind Tunnel Model," Wright Laboratory, WL-TM-92-350-FIBG, September 1992.

13 Marple, S.L. Jr., *Digital Spectral Analysis with Applications*, Prentice-Hall Inc., New York, 1987.

14 James, K.D. and Meyn, L.A.: "Dependence of Integrated Vertical-Tail Buffet Loads For F/A-18 on Sensor Density," SAE Paper 941140, SAE Aerospace Atlantic Comference, April 1994.